Severe arrhythmia disorder caused by cardiac L-type calcium channel mutations

Igor Splawski*†‡§¶, Katherine W. Timothy*†‡§, Niels Decher‖**, Pradeep Kumar‖**, Frank B. Sachse**††, Alan H. Beggs‡,‡‡, Michael C. Sanguinetti‖**, and Mark T. Keating*†‡§

*Howard Hughes Medical Institute, †Department of Cardiology, and ‡‡Genomics Program and Division of Genetics, Children's Hospital, and Departments of ‡Pediatrics and §Cell Biology, Harvard Medical School, Boston, MA 02115; and Departments of ‖Physiology and ††Bioengineering, and **Nora Eccles Harrison Cardiovascular Research and Training Institute, University of Utah, Salt Lake City, UT 84112

Timothy syndrome (TS) is a multisystem disorder that causes syncope and sudden death from cardiac arrhythmias. Prominent features include congenital heart disease, immune deficiency, intermittent hypoglycemia, cognitive abnormalities, and autism. All TS individuals have syndactyly (webbing of fingers and toes). We discovered that TS resulted from a recurrent, *de novo* cardiac L-type calcium channel ($Ca_V1.2$) mutation, G406R. G406 is located in alternatively spliced exon 8A, encoding transmembrane segment S6 of domain I. Here, we describe two individuals with a severe variant of TS (TS2). Neither child had syndactyly. Both individuals had extreme prolongation of the QT interval on electrocardiogram, with a QT interval corrected for heart rate ranging from 620 to 730 ms, causing multiple arrhythmias and sudden death. One individual had severe mental retardation and nemaline rod skeletal myopathy. We identified *de novo* missense mutations in exon 8 of $Ca_V1.2$ in both individuals. One was an analogous mutation to that found in exon 8A in classic TS, G406R. The other mutation was G402S. Exon 8 encodes the same region as exon 8A, and the two are mutually exclusive. The spliced form of $Ca_V1.2$ containing exon 8 is highly expressed in heart and brain, accounting for ≈80% of $Ca_V1.2$ mRNAs. G406R and G402S cause reduced channel inactivation, resulting in maintained depolarizing L-type calcium currents. Computer modeling showed prolongation of cardiomyocyte action potentials and delayed afterdepolarizations, factors that increase risk of arrhythmia. These data indicate that gain-of-function mutations of $Ca_V1.2$ exons 8 and 8A cause distinct forms of TS.

long QT syndrome | Timothy syndrome | CACNA1C

Timothy syndrome (TS) is a multisystem disorder characterized by simple syndactyly and life-threatening cardiac arrhythmias. The first cases of TS were described in 1992 and 1995 as sporadic cases of long QT syndrome, congenital heart disease, and syndactyly (1–3). With time and life-extending therapy it became clear that TS manifests major phenotypic abnormalities in multiple organ systems (4). All TS cases had QT interval prolongation on electrocardiogram, syndactyly, and abnormal teeth and were born bald. Most had arrhythmias, including bradycardia, atrio-ventricular block, torsades de pointes ventricular tachycardia (torsades), and ventricular fibrillation. Ten of 17 TS children died with an average age at death of 2.5 years. Additional common features included congenital heart disease, dysmorphic facial features, myopia, immune deficiency, recurrent infections, intermittent hypoglycemia, and hypothermia. Finally, many TS children had developmental delays, including language, motor, and generalized cognitive impairment. Some did not produce speech sounds during infancy. Significant problems in articulation, reception, and expression were identified. Five children were evaluated for autism, and three met the criteria for this disorder. One TS child met criteria for autism spectrum disorders and one had severe delays in language development. Thus, TS is a complex physiological and develop-

mental disorder affecting multiple organ systems including the heart, digits, and brain.

TS presented as a sporadic trait in all but one family. In that family, two of three siblings were affected. None of the parents in any family were affected. We discovered that TS resulted from an identical, *de novo*, gain-of-function missense mutation in exon 8A of the cardiac L-type calcium channel ($Ca_V1.2$) (4, 5). $Ca_V1.2$ is important for excitation–contraction coupling in the heart. We found that it is also expressed in other tissues including brain, smooth muscle, immune system, teeth, and testis. Functional expression of mutant and WT channels in heterologous systems demonstrated that the causative mutation, G406R, leads to nearly complete absence of voltage-dependent channel inactivation. The resulting inward Ca^{2+} currents likely induce intracellular Ca^{2+} overload in multiple cell types. Thus, abnormal Ca^{2+} signaling is the cause of TS.

An unusual feature of TS was its molecular homogeneity; all cases resulted from the identical, *de novo*, missense mutation G406R in exon 8A. In addition, all cases of TS showed simple syndactyly. Here, we describe two cases of atypical TS (TS2). Both had severe QT interval prolongation, with QT interval corrected for heart rate (QTc) ranging from 620 to 730 ms, and had multiple episodes of arrhythmias. One recently died of torsades and ventricular fibrillation. This individual had many other significant phenotypic abnormalities including severe mental retardation and a skeletal muscle disease known as nemaline myopathy (NM) (5). Neither of these cases had syndactyly. As in TS, we discovered that the phenotype in these individuals resulted from *de novo* missense mutations of $Ca_V1.2$. However, these mutations affect exon 8, not exon 8A. One mutation was analogous to that identified in classic TS, G406R, whereas the other was G402S. As with TS, we found that both mutations caused nearly complete failure of voltage-dependent channel inactivation, leading to maintained inward Ca^{2+} currents.

Materials and Methods

Subject Ascertainment and Phenotypic Analysis. Phenotypic analyses included history, physical examination, electrocardiography, and echocardiography. Informed consent or assent was obtained from individuals or their guardians according to standards established by local institutional review boards. Table 1 gives details of the individual cases.

Table 1. Phenotypic features of TS2

Phenotype	6-year-old female	21-year-old male	TS, %
Skin			
Syndactyly	N	N	100
Severe rashes	Y	n/a	57
Muscoskeletal			
Nemaline myopathy	Y	N	0
Hyper-flexible joints	Y	Y	0
Congenital hip dislocation	Y	N	0
Truncal hypotonia	Y	N	0
Heart			
QT prolongation	Y	Y	100
Arrhythmia			
Multiple cardiac arrests	Y	Y	86
Ventricular tachyarrhythmia	Y	Y	71
Bradycardia, atrio-ventricular block	Y	n/a	94
Torsades	Y	Y	86
Atrial fibrillation	N	Y	0
Hypertrophic cardiomyopathy	Y	Y	50
Patent ductus arteriosus	Y	n/a	59
CNS			
Developmental delays			
Language	Y	N	62
Social	Y	N	54
Gross motor	Y	N	57
Fine motor	Y	N	38
Mental retardation	Y	Y	25
Seizures	Y	n/a	21
Irregular sleep patterns	Y	Y	29
Gastro-intestinal			
Gag reflex	Y	n/a	31
Bloody stools	Y	N	0
Frequent constipation	Y	n/a	33
Cranio-facial			
Flat nasal bridge	Y	Y	83
Large cranium	N	Y	14
Protruding forehead	Y	Y	0
Protruding tongue	Y	N	0
Eyes			
Myopia	n/a	Y	25
Unusual eye movements	Y	N	0
Different size pupils	Y	N	0
Teeth			
Cavities	Y	N	50
Lungs			
Bronchitis	Y	Y	47
Asthma	N	Y	40
Recurrent infections	Y	Y	75

N, absence of phenotype; Y, presence of phenotype; n/a, no data available.

Fig. 1. Dysmorphic facial features, marked QT interval prolongation, arrhythmia, and skeletal muscle defects in affected individuals. (*A–C*) Individual 1 exhibiting dysmorphic facial features including flat nasal bridge, thin upper lip, and protruding tongue. (*D*) Electrocardiogram shows severe QT interval prolongation, causing 2:1 atrio-ventricular block seen as two atrial beats (P-waves) for each ventricular beat (QRS complex). (*E*) Electrocardiogram shows polymorphic ventricular tachycardia for individual 1. (*F*) Frozen section of left quadriceps biopsy stained with modified Gomori trichrome showing rare nemaline rods (indicated by arrows) in scattered myofibers (scale bar, 20 μm). (*G*) Electron micrograph of subsarcolemmal collections of electron dense rods ($\times$17,800). (*H*) Electron micrograph illustrating normal sarcomeric architecture for comparison with *G* ($\times$17,800).

Genotypic and Sequence Analyses. Genomic DNA from peripheral blood lymphocytes or cell lines derived from Epstein–Barr virus-transformed lymphocytes was prepared by using a Puregene DNA isolation kit (Gentra Systems, Minneapolis). Genomic DNA from buccal swabs was prepared by using a QIAamp DNA Mini Kit (Qiagen, Valencia, CA). PCR amplification of Ca$_V$1.2 exons DNA samples and mutational analyses were carried out as described (4, 6). Exons 8 (first) and 8A (second) were designated according to their order in genomic DNA. Oligonucleotides and PCR conditions for the amplification of nebulin exons 145–148, 151–171, 173, and 175–182 were obtained from K. Pelin (University of Helsinki, Helsinki). The 5′ UTR and the entire coding sequence of skeletal muscle α-actin were amplified with four pairs of oligonucleotides:

1F-GGTGGCGCGGAGGGAATG and 1R-TTCTGCCCCG-GAGTCCTTC (amplicon of 223 bp), 2F-TGAGTCTGCGCT-GATGC and 2R-GGGCGGGAGAGGGGG (663 bp), 3F-CCCCCAGCCACTCACTCTC and 3R-GCGGGGAGC-GTGAGCAGA (552), and 4F-AGCTTCTGCTCACGCTCCC and 4R-GTCCTGAGAAGTCGCGTGCT (473 bp). α-Actin oligonucleotides were designed to genomic sequences found in the Celera database by using OLIGO6.6 (Molecular Biology Insights, Cascade, CO). PCR fragments were purified by using a QIAquick PCR purification kit (Qiagen), and sequencing was performed with an Applied Biosystems 3700 automated DNA sequencer.

mRNA Expression and cDNA Analyses. Northern blot analyses were performed by using human 12-lane Multiple Tissue Northern blots I and III (BD Biosciences Clontech). mRNA dot blot analysis was conducted by using the Multiple Tissue Expression Human Array 3 (BD Biosciences Clontech). A 117-bp PCR fragment, amplified from Ca$_V$1.2 cDNA with forward-GATGCAGGACGCTATGGGC and reverse-TGGAAAACT-CTCCGCTCAACA oligonucleotides, was used as a probe for exon 8-containing mRNAs. The fragment was labeled with the Prime-It II labeling kit (Stratagene) using the reverse oligonu-
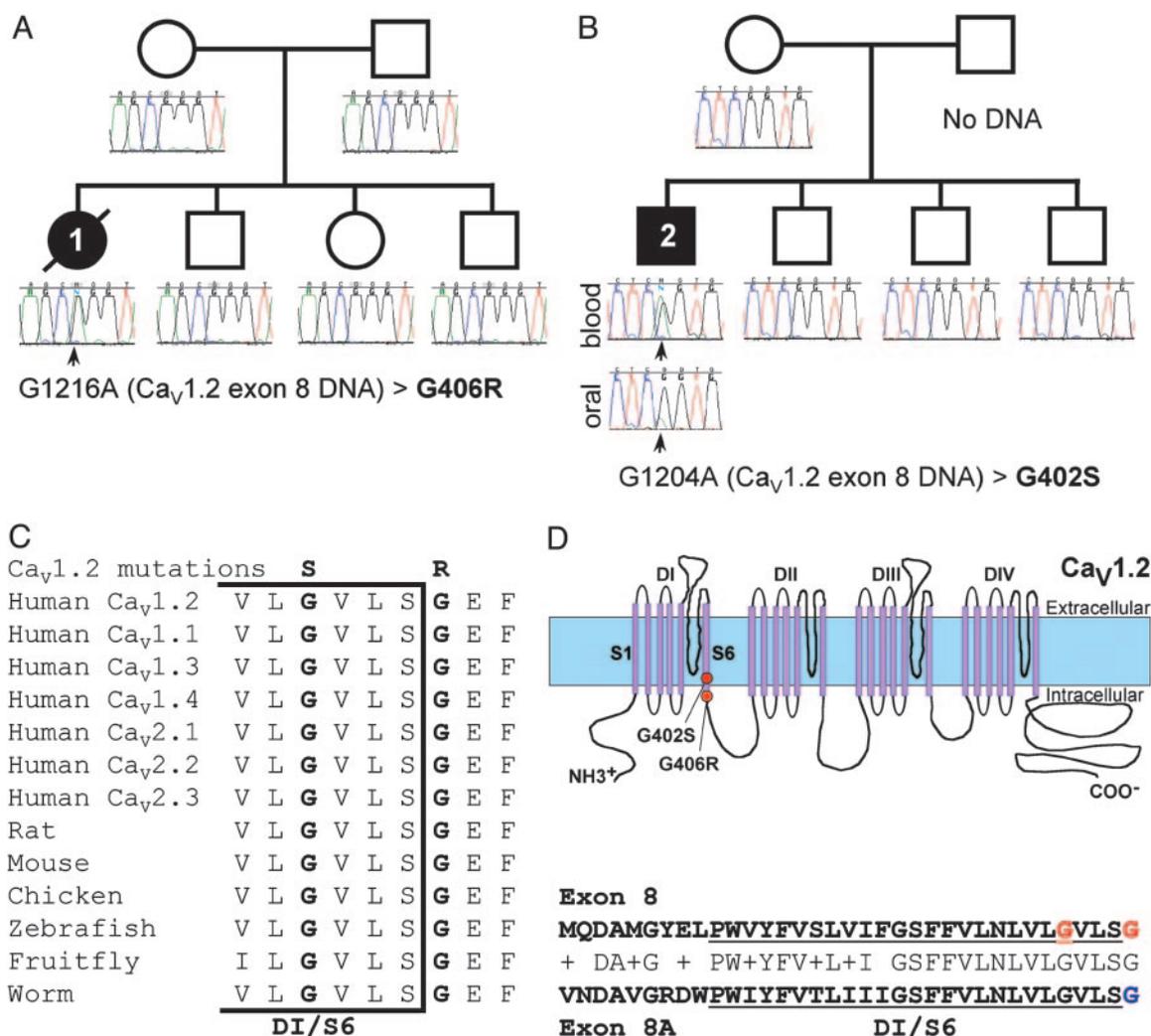
Fig. 2. *De novo* Ca$_V$1.2 mutations cause TS2. (*A*) Pedigree shows sporadic occurrence of the disease phenotype and *de novo* G1216A missense mutation in individual 1. This mutation leads to the substitution of glycine 406 with arginine (G406R) in exon 8. Circles and squares indicate females and males, respectively. Filled and empty symbols denote affected and unaffected individuals, respectively. The individual with a slash is deceased. Sequence tracings were derived from blood DNA samples unless otherwise indicated. (*B*) Pedigree shows sporadic occurrence of the disease phenotype and *de novo* G1204A missense mutation in individual 2. This mutation leads to the substitution of glycine 402 with serine (G402S) in exon 8. The mutant peak (green, arrow) is present in sequence from blood DNA but only a small peak is detected in oral mucosa DNA, indicating mosaicism. Mosaicism may explain the milder phenotype in this individual. (*C*) Amino acid sequence alignment showing conservation of glycine at positions 402 and 406 from multiple species. Bracket indicates the end of the sixth transmembrane segment of domain I (DI/S6). (*D*) (*Upper*) Predicted topology of Ca$_V$1.2, showing the location of the mutations. (*Lower*) Homology of the amino acid sequence of exons 8 and 8A. DI/S6 is underlined. G402 and G406, the amino acids mutated in TS2, are both in exon 8 and are shown in red. G406, mutated in TS, is in exon 8A and is shown in blue. These data indicate that *de novo* missense mutations in Ca$_V$1.2 exon 8 cause severe long QT syndrome and other phenotypic abnormalities.

cleotide instead of the provided random 9-mers. Hybridization and washing conditions followed manufacturer's suggestions. The blots were exposed to film for 3 days.

DNA Constructs for Functional Expression. Full-length human WT Ca$_V$1.2 cDNA (GenBank accession no. AJ224873), cloned in a *Xenopus* (pBluescript) expression vector system, was a generous gift from N. Soldatov (National Institute on Aging, Bethesda). The G402S and G406R mutations were introduced by site-directed mutagenesis using Quikchange (Stratagene).

Ca$_V$β$_{2b}$ and Ca$_V$α$_2$δ$_1$ are the accessory subunits associated with Ca$_V$1.2 in the human heart (7, 8). The rabbit Ca$_V$β$_{2b}$ and Ca$_V$α$_2$δ$_1$ clones used for expression in *Xenopus* oocytes were a kind gift from N. Dascal (Tel Aviv University, Ramat Aviv, Israel).

The full-length clones for all four expression constructs de-

scribed above were sequenced in forward and reverse direction and compared with genomic DNA to ensure that no unintended mutations were present or introduced.

Injection and Solutions for Oocytes. Isolation and injection of *Xenopus laevis* oocytes, and synthesis of capped poly(A) complementary RNA (cRNA) from linearized cDNA templates was performed as described (9). Oocytes were coinjected with cRNAs encoding WT or mutant human Ca$_V$1.2 subunit (11 ng) plus rabbit Ca$_V$β$_{2b}$ (2.7 ng) and rabbit Ca$_V$α$_2$δ$_1$ (2.7 ng) subunits. The extracellular solution contained 40 mM Ba(OH)$_2$, 50 mM NaOH, 1 mM KOH, and 5 mM Hepes (pH 7.4 with methanesulfonic acid, 22–25°C). Niflumic acid (300 μM) was added to the solution to block endogenous Ca^{2+}-activated Cl$^-$ currents (10).

Voltage Clamp and Data Analysis. Ba^{2+} currents through Ca$_V$1.2 channels were recorded from oocytes by using standard two-

microelectrode voltage clamp techniques 2–10 days after injection of cRNA (11, 12). Micropipettes contained 3 M KCl and had resistances of 0.5–1 MΩ. Current–voltage (I–V) relationships were determined by measuring the peak inward current elicited by 2-s test pulses applied in 10-mV increments to potentials ranging from −70 to +40 mV. The holding potential was −80 mV. Currents were filtered at 2 kHz and digitized at 10 kHz. The relative voltage dependence of activation was calculated from normalized peak inward currents (I_{peak}) and the extrapolated reversal potential (E_{rev}) for each oocyte. The voltage dependence of Ba^{2+} current inactivation was determined with a two-pulse protocol. The relative magnitude of inward current elicited during a second pulse (to +10 mV) was plotted as a function of the variable voltage of the conditioning 2-s prepulse. Data were fitted to a Boltzmann function to obtain the half-point ($V_{1/2}$) and slope factor (k) for the relationships describing the voltage dependence of $Ca_V1.2$ activation and inactivation. Data acquisition and analyses were performed by using PCLAMP8 software (Axon Instruments, Union City, CA). Data are presented as mean ± SE (n = number of oocytes).

Cardiac Myocyte Modeling. A model of a human left ventricular myocyte (13) was used to simulate the effects of exon 8 and exon 8A G406R mutations. Channel properties of WT and mutant L-type calcium channels were modeled by adjusting the relative voltage-dependent inactivation function y_∞. The channel descriptions were combined in the myocyte model to reconstruct a heterozygous condition in which the exon 8 containing $Ca_V1.2$ protein represents 77% (38.5% WT, 38.5% G406R) of the total $Ca_V1.2$ protein. In addition, a model was created for a heterozygous condition in which the exon 8A containing $Ca_V1.2$ protein represents 23% (11.5% WT and 11.5% G406R) of the total $Ca_V1.2$ protein (4). A model of spontaneous calcium release from the junctional sarcoplasmic reticulum via ryanodine receptor calcium channels was incorporated in the myocyte model (14). The threshold for spontaneous release of intracellular Ca^{2+} corresponds to 70% of calsequestrin-bound Ca^{2+}.

Simulations with the channel and myocyte models were carried out with the Euler method for numerical integration of ordinary differential equations (15). For simulations with the myocyte model, the temporal discretization for solving the equations was adapted for various components (e.g., the Na channel description) of the model.

Results

TS2. A Caucasian individual (individual 1) came to medical attention at 25 weeks gestation because of bradycardia (heart rate of 60 bpm) and 2:1 atrio-ventricular conduction (Fig. 1). Additional findings included biventricular hypertrophy and moderate biventricular dysfunction. The infant girl was born by cesarean section because of severe bradycardia at 38 weeks gestation. At birth, the infant was alternating between normal conduction and 2:1 atrio-ventricular block and had marked prolongation of the QT interval (QTc of 730 ms). An implantable pacemaker was placed in an effort to improve cardiac conduction. However, ventricular pacing was not safe as it consistently led to the development of torsades. Instead, the atrium was paced at 140 bpm with a ventricular response of 70 bpm that was tolerated. The infant was discharged from the hospital with 24-h nursing care and monitoring.

At 4 months of age the child experienced an episode of cyanosis and apnea during feeding. The infant was taken by ambulance to the hospital. She underwent electro-cardioversion six times en route to and during hospitalization. One episode required resuscitation. Medications included propranolol, enalapril, and mexilitine. Evidence of biventricular hypertophy was noted. Arrests did not respond to i.v. magnesium, i.v. lidocaine, or cardioversion. Increasing the serum potassium concentration
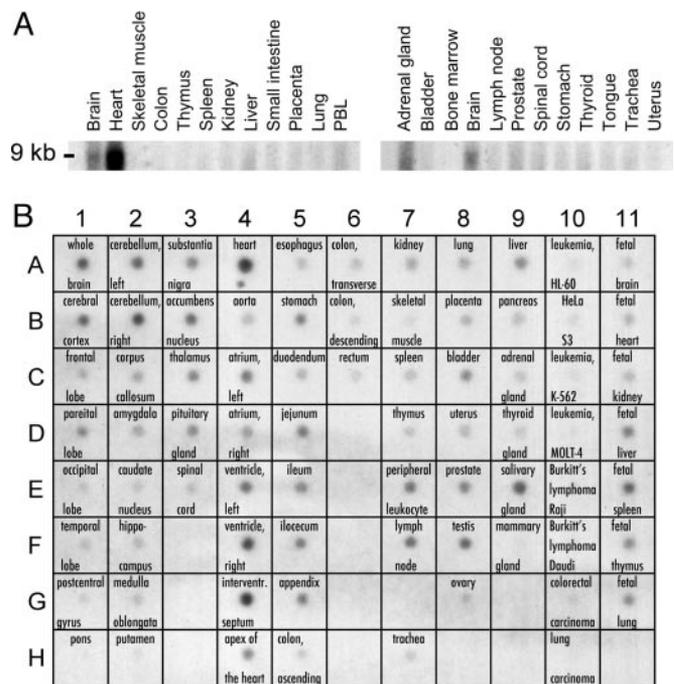

Fig. 3. The $Ca_V1.2$ exon 8 splice variant is highly expressed in heart and brain. (*A*) Human Northern blot analyses show expression of $Ca_V1.2$ exon 8 in brain, heart, and other tissues. (*B*) mRNA dot blot demonstrates expression of $Ca_V1.2$ exon 8 in multiple fetal and adult tissues, including many regions of the brain.

did not change the QT interval. Two weeks later cervical sympathetic ganglionectomy and a ventricular pacemaker placement were completed in an attempt to reduce arrhythmias. Neither intervention was effective.

This individual also suffered from bilateral congenitally dislocated hips and joint hyperextensibility. A skeletal muscle biopsy at 5 months demonstrated mild variation in fiber size with minimal fiber type 1 atrophy and occasional smaller fibers with collections of nemaline rods (Fig. 1*F*). A pathological diagnosis of NM was confirmed by identification of nemaline rods by electron microscopy (Fig. 1 *G* and *H*), which also revealed mild focal increases in glycogen content. Mitochondria were morphologically normal. By age 6, it became apparent that the patient suffered from a discrepancy of body development. Although her upper body appeared normal for her age, her lower body had an appearance typical of a 2- or 3-year-old. Notable facial characteristics included a protruding forehead, depressed nasal bridge, and protruding tongue. Dental enamel was poorly developed, and severe caries prompted the extraction of most teeth. Significant T wave alternans and torsades were documented during anesthesia.

The child had seizures with increasing frequency. Other neurological observations included frequent startle reflexes, static encephalopathy, and irregular sleep patterns. Upon examination, no developmental regression was noticed. At age 6 the child could not hold her head up without support, but she could roll over. She could not hold a cup or utensils. The child smiled sometimes and made some sounds, but words were not recognizable. At age 6, she died of ventricular fibrillation. No family members had any of the phenotypic features identified in individual 1.

A Caucasian boy (individual 2) was born by caesarian section at 38 weeks gestation. No cardiac or health problems were noted at birth or during infancy. The child grew normally, achieving all developmental milestones within normal time frames. However, he had a cardiac arrest at the age of 4 years while climbing onto
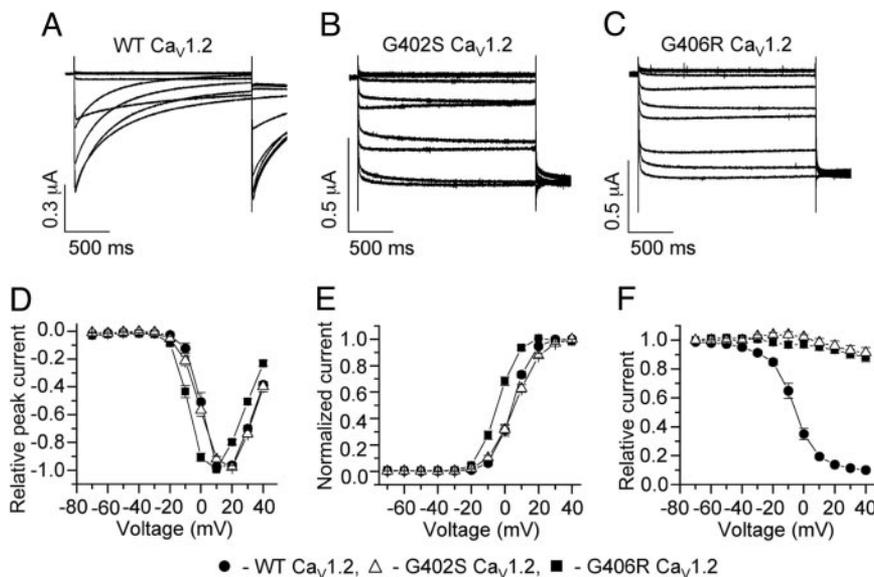
Fig. 4. Mutations of $Ca_V1.2$ exon 8 cause nearly complete absence of voltage-dependent channel inactivation. (*A–C*) WT (*A*), G402S (*B*), and G406R (*C*) $Ca_V1.2$ channel currents were recorded from *Xenopus* oocytes in response to voltage pulses applied in 10-mV increments from -70 to $+40$ mV, second pulse to $+10$ mV. External solution contained 40 mM $BaCl_2$ to eliminate Ca^{2+}-dependent inactivation of $Ca_V1.2$ channels. Note the lack of current inactivation for mutant channels compared with WT channel currents. (*D*) G406R channels have similar Ba^{2+} current–voltage (*I–V*) relationship compared with WT. (*E*) Voltage dependence of Ba^{2+} current activation for WT ($V_{1/2} = 4.5 \pm 0.1$ mV; $k = 5.5 \pm 0.1$ mV; $n = 7$), G402S ($V_{1/2} = 6.2 \pm 0.1$ mV; $k = 7.5 \pm 0.1$ mV; $n = 14$), and G406R ($V_{1/2} = -4.4 \pm 0.3$ mV; $k = 5.4 \pm 0.2$ mV; $n = 14$). (*F*) Voltage dependence of Ba^{2+} current inactivation for WT ($V_{1/2} = -6.6 \pm 0.4$ mV; k $= 7.6 \pm 0.4$ mV; $n = 8$) and mutant $Ca_V1.2$ channels. The minimum value for relative inactivation was 0.10 ± 0.01 for WT ($n = 8$), but 0.88 ± 0.03 for G406R ($n = 15$) and 0.91 ± 0.04 for G402S ($n = 6$), indicating nearly complete absence of voltage dependence of inactivation.

a trampoline. The child's teacher performed CPR, and he was taken to the hospital where a diagnosis of long QT syndrome was made. Over the next 6 years, the child experienced at least three additional episodes of cardiac arrest, all triggered by auditory stimuli. A pacemaker was implanted. At age 11, he suffered a cardiac arrest after therapy with Bactrim (Sulfamethoxazole and Trimethoprim) for a nasal infection. He was then in a coma for 2 weeks. Although rehabilitation helped the child regain physical, mental, and social abilities, significant brain damage remained. At that time, an automatic cardiac defibrillator was placed that has subsequently fired >20 times. At present, he is experiencing cardiac arrhythmias once a week, always at night and associated with night terrors. Caregivers have also noted signs of depression and obsessive-compulsive behavior.

De Novo Missense Mutations in $Ca_V1.2$ Cause TS2. In a previous study, we showed that a recurrent *de novo* missense mutation in $Ca_V1.2$ caused TS (4). We hypothesized that mutations in this gene could be associated with other forms of this disorder. We screened all 50 exons of $Ca_V1.2$ in 324 individuals with arrhythmia. Two disease-associated mutations were identified. Analysis of exon 8 revealed a G1216A transition in DNA samples from individual 1 (Fig. 2*A*). This transition led to the substitution of glycine with arginine at residue 406 (G406R). A G1204A transition in the same exon was identified in individual 2, causing a glycine-to-serine change at position 402 (G402S, Fig. 2*B*). Both amino acids (G406 and G402) are completely conserved in other voltage-dependent calcium channels of multiple species, ranging from worms to humans (Fig. 2*C*), and are located at the C-terminal end of the sixth transmembrane segment of domain I (DI/S6, Fig. 2*D*). Neither mutation was identified in 182 ethnically matched control samples (364 chromosomes). Mutational analysis of additional family members, including parents, failed to reveal mutations in $Ca_V1.2$. The relatively milder phenotype of individual 2 led us to hypothesize that he might be a mosaic. To test the hypothesis, we obtained DNA from oral

mucosa. A mutant peak for the missense mutation was observed. This mutant peak, however, was much smaller compared with the mutant peak detected in blood DNA (Fig. 2*B*). This finding indicates that the mutation arose during development and is present only in a subset of cells. Thus, the phenotype in these two probands resulted from *de novo* mutations in $Ca_V1.2$.

To test the possibility that the NM present in individual 1 could have been caused by mutations in genes previously implicated in this disorder, we examined the entire sequence of skeletal muscle α-actin (*ACTA1*) and 35 exons of nebulin (*NEB*) that contain all previously identified mutations associated with
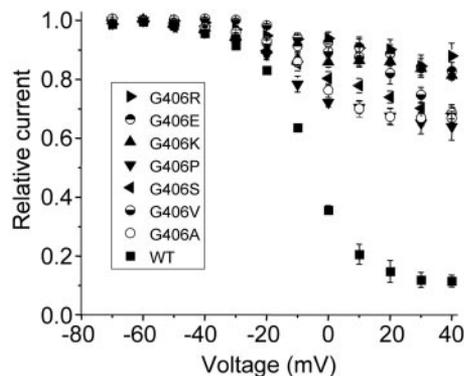
Fig. 5. Glycine is a critical amino acid at position 406 of $Ca_V1.2$. Voltage dependence of inactivation for WT and mutant exon 8 $Ca_V1.2$ channels were determined in *Xenopus* oocytes by measuring the peak amplitude of current evoked during a pulse to $+10$ mV that followed a 2-s conditioning pulse applied to a variable potential. Currents were normalized and plotted as a function of the conditioning potential. External solution contained 40 mM $BaCl_2$ to eliminate Ca^{2+}-dependent inactivation. WT, $n = 6$; G406R, $n = 10$; G406E, $n = 11$; G406K, $n = 9$; G406P, $n = 8$; G406S, $n = 8$; G406V, $n = 6$; G406A, $n = 11$.

Fig. 6. Computer modeling revealed prolonged action potentials, altered intracellular calcium handling, and DADs induced by $Ca_V1.2$ mutations. (*A*) Simulated voltage dependence of L-type calcium channel current inactivation for WT (black), G406R (green), WT/exon 8 G406R heterozygotes (red), and WT/exon 8A G406R heterozygotes (blue). The relative voltage-dependent inactivation was plotted as a function of V_m. (*B*) Intracellular calcium transients during a simulated action potential. The peak of the transient was increased by 29% in WT/exon 8 G406R heterozygotes compared with 7% in WT/exon 8A G406R, because the exon 8 splice variant expression was assumed to predominate in the heart with a ratio ≈3.5:1. (*C*) Cardiac action potentials were prolonged by 30% in WT/exon 8 G406R compared with 8% prolongation in WT/exon 8A G406R heterozygotes. (*D–F*) Transients of $[Ca^{2+}]_{JSR}$ (*D*), $[Ca^{2+}]_i$ (*E*), and V_m (*F*) were calculated for a stimulus frequency of 3 Hz. The last three action potentials of 3-Hz pacing were followed by a pause. During this pause, exon WT/exon 8A G406R led to a DAD after 509 ms with a peak voltage of −54 mV; WT/exon 8 G406R led to a triggered action potential after 423 ms with a peak voltage of 26 mV. In this model, DADs result from spontaneous release of Ca^{2+} from the sarcoplasmic reticulum. Experimental studies of cardiac myocytes have shown that DADs result from Ca_i overload and subsequent activation of the Na/Ca exchanger, and to a lesser extent, a Ca_i-activated cation-nonselective conductance and a Ca_i-activated Cl^- conductance (23–25).

NM. These two genes are likely responsible for ≈75% of NM cases (5). Sequence analysis did not detect any mutations.

$Ca_V1.2$ Exon 8 Is Highly Expressed in Heart and Brain. In $Ca_V1.2$, transmembrane segment 6 of domain I (D1/S6) can be encoded by two mutually exclusive exons, 8 and 8A. We previously determined the tissue and cellular distribution of the alternatively spliced form containing exon 8A (4). To determine the pattern of expression of the dominant alternatively spliced form of $Ca_V1.2$ containing exon 8, we used this exon as a probe for Northern and dot blot analyses. In adult and fetal samples, exon 8 was expressed in multiple tissues. Exon 8 is very highly expressed in the heart (Fig. 3*A*). This exon is also expressed at lower levels in the brain and adrenal gland. Within the brain, dot blot analysis showed that exon 8 is expressed in cerebellum, cerebral cortex, substantia nigra, accumbens nucleus, thalamus, and pituitary gland. It is also expressed in stomach, jejunum, ileum, bladder, prostate, testis, peripheral leukocyte, lymph node, liver, and salivary gland. Fetal organs that show expression include brain, heart, liver, spleen, thymus, and lung. By comparison, exon 8A expression is less impressive in heart and brain, adrenal gland, salivary gland, peripheral leukocyte, and lymph node. On the other hand, exon 8A expression was higher in organs with smooth muscle including the aorta, bladder, and

uterus (4). We previously determined that exon 8 represents ≈80% of mRNAs in heart and brain (4). In summary, these data indicate that $Ca_V1.2$ exon 8 is highly expressed in heart and brain, consistent with the severe cardiac and cognitive defects associated with the two mutations described above.

G402S and G406R Mutations Impair Channel Inactivation. To determine the molecular consequences of the G402S and G406R mutations, we heterologously expressed WT and mutant forms of the $Ca_V1.2$ channel in *Xenopus* oocytes. Oocytes were injected with cRNA encoding $Ca_V1.2$ and its accessory subunits $Ca_V\beta_{2b}$ and $Ca_V\alpha_2\delta_1$. We recorded WT and mutant channel activity by using Ba^{2+} (40 mM) as a charge carrier. Ba^{2+} currents inactivate much slower than Ca^{2+} currents, because in the absence of extracellular Ca^{2+}, channel inactivation almost entirely depends on transmembrane voltage (V_m) (16). Compared with WT channels (Fig. 4*A*), the time-dependent inactivation of mutant channels was dramatically reduced by both mutations (Fig. 4 *B* and *C*). WT and G402S channels had a similar *I–V* relationship and voltage dependence of current activation, whereas the relationships for G406R channels were shifted by −9 mV (Fig. 4 *D* and *E*). Next, we determined the voltage dependence of inactivation by using 2-s conditioning pulses as described in *Materials and Methods*. Whereas WT channels inactivated 90%

Fig. 7. Transient changes in stimulation frequency lead to electrophysiological instabilities in myocytes harboring Ca$_V$1.2 channel mutations. In this simulation, the stimulus frequency was increased from 2.5 to 3 Hz at time 0 s. The myocyte was then stimulated at 3 Hz for a variable duration (*t*), followed by a pause. The peak values of [Ca^{2+}]$_{JSR}$ (*A*), [Ca^{2+}]$_i$ (*B*), and V$_m$ (*C*) as well as the start time of spontaneous calcium release (*D*) were determined during the pause. The start time is specified relative to the time of the last stimulus. In the transitional phase, myocytes with WT/exon 8A G406R Ca$_V$1.2 showed subthreshold DADs between *t* = 9 and 77 s. With longer times (*t* >77 s) the DAD triggered an action potential. Myocytes with WT/exon 8 G406R Ca$_V$1.2 also exhibited DADs, which were sporadic for *t* <82 s. Only some of these DADs triggered action potentials (e.g., at *t* = 67 s). WT myocytes never showed DADs. Together, these simulations predict that the Ca$_V$1.2 mutations promote electrophysiological instability that could induce lethal arrhythmia in response to relatively minor changes in heart rate.

after a conditioning pulse to +30 mV, G406R and G402S channels inactivated 12% and 9%, respectively, at the same potential (Fig. 4*F*). These data demonstrate that the G402S and G406R mutations greatly reduce the extent of voltage-dependent Ca$_V$1.2 channel inactivation and produce maintained inward Ca^{2+} currents. Thus, the G402S and G406R mutations have a gain-of-function effect on Ca$_V$1.2 calcium channels.

The G406R-induced inhibition of voltage-dependent channel inactivation was presumably caused by impaired function normally provided by glycine at position 406. To determine the importance of the glycine residue we mutated G406 to several other residues. The substitutions included another basic residue (lysine), an acidic residue (glutamic acid), a polar but uncharged residue (serine), small hydrophobic residues (alanine and valine), and another distinct amino acid (proline). Despite the differences in the physicochemical nature of the side chains of

these residues, each of the substitutions inhibited voltage-dependent inactivation (Fig. 5). These data indicate that normal inactivation is uniquely provided by glycine at position 406 in the Ca$_V$1.2 channel.

Ca$_V$1.2 Mutations Prolong Simulated Action Potentials. Two prominent features present in both TS2 individuals are severe prolongation of the QT interval and life-threatening arrhythmias. Reduced Ca$_V$1.2 channel inactivation should prolong the inward (membrane depolarizing) Ca^{2+} current during the plateau phase and delay cardiomyocyte repolarization. As the effect of the G402S and G406R (exon 8) mutations on channel function was similar, we chose to simulate the effect of the G406R mutation and compare it with the effect of the G406R mutation identified in exon 8A (4).

We previously determined that 77% of Ca$_V$1.2 channels in the heart contained exon 8 and 23% contained exon 8A (4). Thus, in the heterozygous state, 38.5% of Ca$_V$1.2 channels carry the exon 8 mutation in TS2 cases and 11.5% carry the exon 8A mutation in TS cases. We assumed these ratios to simulate the altered L-type calcium channel inactivation (Fig. 6*A*) caused by the mutations in a dynamic model of a human ventricular myocyte (13). The mutations increased peak concentration of intracellular Ca^{2+} (Fig. 6*B*) and prolonged action potential duration (Fig. 6*C*) when the model cell was paced at a frequency of 1 Hz.

Transients of junctional sarcoplasmic reticulum calcium concentration ([Ca^{2+}]$_{JSR}$, Fig. 6*D*), intracellular calcium concentration ([Ca^{2+}]$_i$, Fig. 6*E*), and V$_m$ (Fig. 6*F*) were calculated for a myocyte harboring the exon 8 or exon 8A mutation and paced at a stimulus frequency of 3 Hz. Cessation of the stimuli led to delayed afterdepolarizations (DADs) after ≈0.5 s for exon 8A G406R and triggered an action potential for exon 8 G406R (Fig. 6*F*). DADs or triggered excitations are known to be arrhythmogenic (17).

Instability in [Ca^{2+}]$_{JSR}$, [Ca^{2+}]$_i$, and V$_m$ could be induced by an abrupt change in stimulation rate. In Fig. 7, at *t* = 0 s, the stimulus rate was switched from 2.5 to 3 Hz, and myocytes were electrically activated at the higher rate for 1–300 additional cycles. The peak values of [Ca^{2+}]$_{JSR}$, [Ca^{2+}]$_i$, and V$_m$ after cessation of each train of electrical stimulations were determined and plotted in Fig. 7 *A–C*. The transitional phase showed significant alternans with DADs that could sometimes trigger an action potential for the exon 8 G406R myocyte. In contrast, the DADs for the exon 8A G406R myocyte were mostly subthreshold for triggering of an action potential. These simulations predict that the exon 8 mutation G406R (same for G402S) causes marked prolongation of cardiac action potentials and DADs, consistent with the severe QT interval prolongation and high risk of arrhythmia in TS2 individuals. The exon 8A mutation is predicted to cause less prolongation of the action potential and electrical alternans but can also induce arrhythmia.

Discussion

We conclude that Ca$_V$1.2 dysfunction causes severe arrhythmia syndrome, TS2. In this study, *de novo* missense mutations G402S and G406R arose in Ca$_V$1.2 exon 8, the dominant splice variant in the heart and brain. By contrast, TS results from the identical G406R mutation in Ca$_V$1.2 exon 8A, a splice variant that represents ≈20% of cardiac mRNAs. Consistent with this finding, TS individuals had an average QTc of 580 ms, multiple arrhythmias were rare, and most arrhythmias were associated with medications and/or anesthesia. TS2 patients, however, had an average QTc of 640 ms and multiple episodes of unprovoked arrhythmia. As with TS, the mechanism of arrhythmia is reduced Ca$_V$1.2 channel inactivation, leading to maintained depolarizing Ca^{2+} currents during the plateau phase of the cardiac action potential. There is

relatively little outward current during the plateau phase, so even modest changes in inward calcium current lead to significant QT interval prolongation. This prolongation, in turn, leads to increased risk of spontaneous, abnormal secondary depolarizations (afterdepolarizations), arrhythmia, and sudden death.

A cardinal feature of TS is simple syndactyly; 100% of cases showed this feature. Neither of the cases presented here had syndactyly. It is likely that this difference results from differential expression of exons 8 and 8A. Other major phenotypic differences between TS and the cases presented here are the severity of the CNS defects in individual 1 (G406R exon 8). Presumably these defects happen because exon 8 represents ≈80% of the $Ca_V1.2$ mRNAs in the brain. The fact that case 2 had relatively mild CNS features (before arrhythmia-induced brain injury) might be because this individual is a mosaic. We previously identified mosaicism in individuals with exon 8A mutations who also had milder or normal phenotypes.

The skeletal myopathy in individual 1 may not be a direct consequence of the $Ca_V1.2$ G406R mutation. Expression of $Ca_V1.2$ in skeletal muscle is low. Furthermore, exon 8A, not exon 8, is the dominant skeletal muscle exon with a ratio of ≈20:1 in both fetal and adult skeletal muscle (I.S., unpublished observations). Skeletal myopathy is not a major feature of TS, which is caused by $Ca_V1.2$ exon 8A mutation. One possible explanation for this apparent paradox may be that individual 1 was immobilized because of severe CNS defects. It is known that immobilization can cause nemaline rod formation (18).

The mutations described here are located in CpG dinucleotides. Assuming the mutation occurred on the noncoding strand, in both cases the mutation was a CpG to TpG. CpG-to-TpG change is caused by the deamination of a methylated cytosine and is the most common spontaneous mutation in biology (19, 20). Transition from C to T would result in the observed G-to-A change on the coding strand in a subsequent cycle of DNA replication.

Substitution of G406 with several different residues disrupted $Ca_V1.2$ channel inactivation similar to that induced by G406R that caused TS2. This finding indicates that glycine is required at position 406 and is also likely required at position 402. Glycine can act as a hinge point within an α-helical structure of proteins. Based on an x-ray crystallographic structure, opening of the MthK bacterial channel occurs when the pore-forming inner α-helix bends at a highly conserved glycine residue (21). A glycine residue in a homologous position is located in the S6 transmembrane domain of most potassium channels where it, too, may perform as the hinge for the activation gate (22). We suggest that G406 (and perhaps G402) acts like a hinge for the intracellular, voltage-dependent inactivation gate of $Ca_V1.2$ that closes in response to membrane depolarization and is distinct from the inactivation gating mechanism that depends on $[Ca^{2+}]_i$ (16).

In summary, we have discovered two additional missense mutations in the S6 segment of domain I of $Ca_V1.2$ that cause TS2. These findings confirm the importance of voltage-dependent inactivation of L-type calcium channels for maintenance of a normal Ca^{2+} homeostasis in multiple organs.

1. Reichenbach, H., Meister, E. M. & Theile, H. (1992) *Kinderarztl Prax* **60,** 54–56.
2. Marks, M. L., Trippel, D. L. & Keating, M. T. (1995) *Am. J. Cardiol.* **76,** 744–745.
3. Marks, M. L., Whisler, S. L., Clericuzio, C. & Keating, M. (1995) *J. Am. Coll. Cardiol.* **25,** 59–64.
4. Splawski, I., Timothy, K. W., Sharpe, L. M., Decher, N., Kumar, P., Bloise, R., Napolitano, C., Schwartz, P. J., Joseph, R. M., Condouris, K., *et al.* (2004) *Cell* **119,** 19–31.
5. Sanoudou, D. & Beggs, A. H. (2001) *Trends Mol. Med.* **7,** 362–368.
6. Splawski, I., Timothy, K. W., Vincent, G. M., Atkinson, D. L. & Keating, M. T. (1997) *N. Engl. J. Med.* **336,** 1562–1567.
7. Colecraft, H. M., Alseikhan, B., Takahashi, S. X., Chaudhuri, D., Mittman, S., Yegnasubramanian, V., Alvania, R. S., Johns, D. C., Marban, E. & Yue, D. T. (2002) *J. Physiol. (London)* **541,** 435–452.
8. Arikkath, J. & Campbell, K. P. (2003) *Curr. Opin. Neurobiol.* **13,** 298–307.
9. Goldin, A. L. (1991) *Methods Cell Biol.* **36,** 487–509.
10. White, M. M. & Aylwin, M. (1990) *Mol. Pharmacol.* **37,** 720–724.
11. Stuhmer, W. (1992) *Methods Enzymol.* **207,** 319–339.
12. Sanguinetti, M. C., Jiang, C., Curran, M. E. & Keating, M. T. (1995) *Cell* **81,** 299–307.
13. Iyer, V., Mazhari, R. & Winslow, R. L. (2004) *Biophys. J.* **87,** 1507–1525.
14. Luo, C. H. & Rudy, Y. (1994) *Circ. Res.* **74,** 1071–1096.
15. Press, W. H., Teukolsky, S. A., Vetterling, W. T. & Flannery, B. P. (1992) *Numerical Recipes in C* (Cambridge Univ. Press, Cambridge, U.K.).
16. Lee, K. S., Marban, E. & Tsien, R. W. (1985) *J. Physiol. (London)* **364,** 395–411.
17. January, C. T., Chau, V. & Makielski, J. C. (1991) *Eur. Heart J.* **12,** Suppl. F, 4–9.
18. Baranska, B., Kujawa, M. & Szulborski, K. (1999) *Folia Morphol. (Warsz)* **58,** 207–214.
19. Cooper, D. N. & Youssoufian, H. (1988) *Hum. Genet.* **78,** 151–155.
20. Vitkup, D., Sander, C. & Church, G. M. (2003) *Genome Biol.* **4,** R72.
21. Jiang, Y., Lee, A., Chen, J., Cadene, M., Chait, B. T. & MacKinnon, R. (2002) *Nature* **417,** 523–526.
22. Shealy, R. T., Murphy, A. D., Ramarathnam, R., Jakobsson, E. & Subramaniam, S. (2003) *Biophys. J.* **84,** 2929–2942.
23. Giles, W. & Shimoni, Y. (1989) *J. Physiol. (London)* **417,** 465–481.
24. Kass, R. S., Tsien, R. W. & Weingart, R. (1978) *J. Physiol. (London)* **281,** 209–226.
25. Zygmunt, A. C., Goodrow, R. J. & Weigel, C. M. (1998) *Am. J. Physiol.* **275,** H1979–H1992.